Directed Assembly

DOI: 10.1002/anie.201202113

Signatures of the Rayleigh-Plateau Instability Revealed by Imposing Synthetic Perturbations on Nanometer-Sized Liquid Metals on Substrates**

*Jason Fowlkes, Scott Horton, Miguel Fuentes-Cabrera, and Philip D. Rack**

Multiscale patterning must be realized to harness the collective action of precisely arrayed nanoscale ensembles over practical meso- and microscales.[1] Plasmonic nanohole-based microlenses[2] and metal nanoparticle necklaces[3] as well as magnetic nanodot[4] and sensor[5] arrays have demonstrated the advantages of multiscale patterning. Self- and directed assembly methods hold promise toward achieving arrays of nanoparticles with both precise interparticle spacing and tailored nanoparticle shape. Recently, in a step towards active assembly, we used electron beam lithography (EBL) to define initial conditions for assembly, which was subsequently activated by pulsed laser melting; the free-energy landscape is thus guided toward lower energy with enhanced fidelity and precision relative to natural self-assembly pathways. Additionally, the melting and re-solidification acts to smooth out high-frequency surface defects, as demonstrated by Chou and Xia.[6] Ultraviolet nanosecond laser pulses are ideal for melting, causing hydrodynamically driven smoothening while keeping substrate heating brief. Depending on the liquid geometry, physical instabilities may propagate which destabilize the liquid, forming nanodroplets. These droplets re-solidify as nanoparticles/nanocaps.

Recently, a large number of publications[7] have demonstrated the assembly of metallic nanoparticle arrays by the amplification of unstable waves on liquid metal surfaces. The unstable wave spectrum is best expressed using a dispersion curve where the growth rate of a given surface mode is expressed as a function of its wavelength or wavevector. Various instabilities, such as the so-called spinodal[8] or Rayleigh-plateau (RP)[9] varieties, have signature dispersion curves reflecting the underlying physics that selects the propagating modal distribution. In the case of the RP instability of a fluid jet, capillary and inertial forces govern the jet breakup. For a fluid jet supported on a substrate (hereafter referred to as a rivulet), a modified RP instability[10] ensues where the substrate–rivulet interaction potential, that is, the wetting angle/spreading parameter,[11] must also be considered. Recently, we have shown, both experimentally and computationally, that for the patterning of unstable varicose modes, synthetic perturbations in nano-/microscale metallic films prior to dewetting can significantly reduce the variation in final nanoparticle spacing by driving a single unstable mode on the jet surface.

Herein, we report our investigation of the nanometer-scale (sub-10 nm) dewetting of 10 Å thick liquid copper thin films supported on graphite substrates using molecular dynamics (MD) simulations. We interpret the MD results within the context of the RP model describing fluid rivulet breakup, with the hope of determining whether the model applies at the nanoscale, and moreover how influential stochastic fluctuations are at the atomic scale. In previous studies, Moseler and Landmann[12a] and Eggers[12b] compared MD and continuum approaches and identified the importance of adding stochastic fluctuations to a physical hydrodynamic model to replicate nanoscale fluid jet destabilization in vapor. The goal is to investigate whether RP fluid jet destabilization, affected by the fluid–substrate interaction, can be adequately captured using MD simulations. We also aimed to investigate the "scalability" of self- and directed assembly of nanoparticle chains by natural RP instabilities and by patterned synthetic perturbations,[7a] and to establish whether this proposal for assembly works at the nanometer scale.

We used the model suggested by Brochard-Wyart and Redon[10c] to explore the influence that the substrate has on the RP instability. While the original RP model treated the specific case of a fluid jet suspended in vacuum/vapor, the liquid–substrate interaction was included by Brochard-Wyart and Redon, where it was shown that the liquid–substrate interaction controls the contact angle of the liquid rivulet on the substrate. The modified analytical expression was used to generate a liquid copper–graphite dispersion plot (that is, perturbation growth rate versus wavelength) for the relevant thin film geometry used in our MD simulations. Based on this

[*] Dr. J. D. Fowlkes, S. R. Horton, Dr. M. Fuentes-Cabrera, Prof. P. D. Rack
Center for Nanophase Materials Sciences
Oak Ridge National Laboratory, Oak Ridge, TN 37831-6493 (USA)
E-mail: prack@utk.edu
Prof. P. D. Rack
Materials Science and Engineering Department
The University of Tennessee, Knoxville, TN 37996-2200 (USA)
S. R. Horton
University of Delaware, Newark, DE 19716 (USA)

[**] J.D.F, P.D.R., and M.F.C. acknowledge support from the U.S. Department of Energy, Basic Energy Sciences, Materials Sciences and Engineering Division for supporting the portions of this work related to the design of molecular dynamics computational experiments and the analysis/models describing the results. M.F.C. acknowledges the computational resources of the UT/ORNL National Institute for Computational Sciences. S.R.H. was supported by an appointment under the Higher Education Research Experience (HERE) program, administered by the Oak Ridge Institute for Science and Education under contract number DE-AC05–06OR23100 between the U.S. Department of Energy and Oak Ridge Associated Universities.

Supporting information for this article is available on the WWW under http://dx.doi.org/10.1002/anie.201202113.

dispersion relation, perturbation wavelengths were selected to pattern thin film strip edges that would promote stabilization and destabilization of the liquid copper rivulet supported on the graphite substrate. Following MD simulations, the stability predictions provided by the analytical model were compared with the MD results; specifically the dynamics/evolution of the liquid metal nanostructures were studied and the correlation between original nanostructures and the final droplet locations were deduced.

Consistent with our previous work, MD simulations were performed using a starting geometry of a liquid Cu thin film strip supported on graphite. Figure 1a shows this geometry for the specific case where an imposed varicose synthetic perturbation was applied. Straight-edged, thin film strips were also studied, and for the purpose of context, these MD simulations will be discussed later (what we refer to as the self-assembly case). The phrase "directed assembly" was used when referring to a thin film strip with an edge perturbation. The choice of the thin film strip geometry, as well as other morphology features demonstrated in Figure 1, have relevance to our current experimental method, which is briefly described in the Supporting Information, S1.

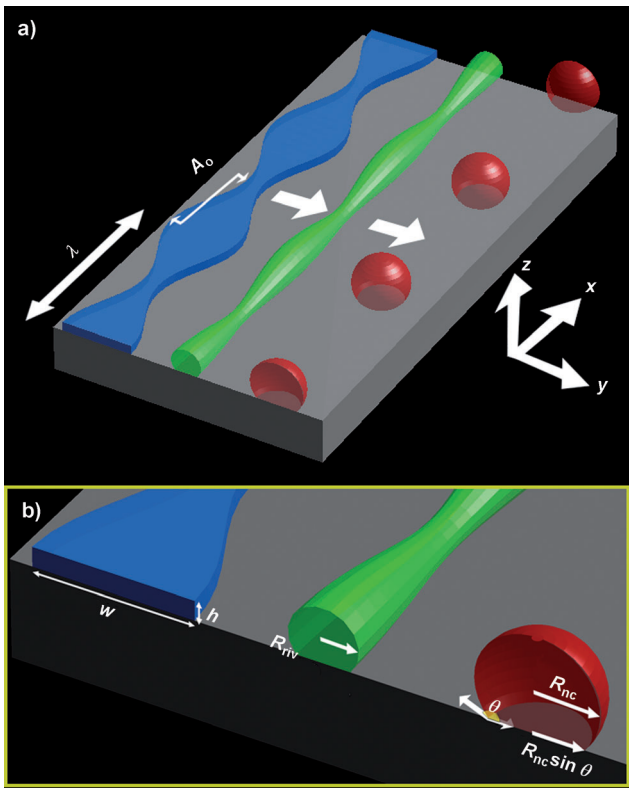

Figure 1. The conversion of the thin film strip geometry (blue) into a rivulet (green) upon dewetting, followed by a linear array of nanodroplets (red), which are in phase with the original strip. A pair of sinusoidal perturbations located on the strip edges with phase difference π, wavelength λ, and amplitude A_o form the varicose perturbation. Once the rivulet morphology forms, the perturbation either decays (stable, $\lambda < \lambda_c$) or grows (unstable, $\lambda > \lambda_c$) according to the substrate-modified Rayleigh-plateau instability. The case of growth is shown: an unstable surface mode destabilizes the rivulet and breakup ensues. b) Critical geometric parameters: height h, width w, rivulet radius R_{riv}, rivulet contact angle θ_{riv}, nanocap radius R_{nc}, contact radius $R_{nc}\sin\theta$, and wetting angle θ.

MD simulations of the straight-edge film strips distinctly reveal the retraction/dewetting, rivulet formation, and breakup as designed. Figure 2a (left column) shows a top-down image of the strip at $t = 0$ ps. We define the straight edges case as a self-assembly process for the following reason. Initially the straight-edge thin film strip dewets/retracts, forming the rivulet morphology (Figure 2b, left). Once a rivulet forms, the natural evolution of surface waves dictates the breakup of the rivulet, and the only control exerted over the breakup was the original definition of the rivulet diameter from the thin film strip height h and width w. In this case, the rivulet radius of 11.7 Å was set by the initial thin film strip height (10 Å) and width (40 Å; Figure 1b) according to equality of cross-sectional areas; $h \times w = R_{riv}{}^2 * (\theta_{riv} - \sin\theta_{riv} \times \cos\theta_{riv})$.

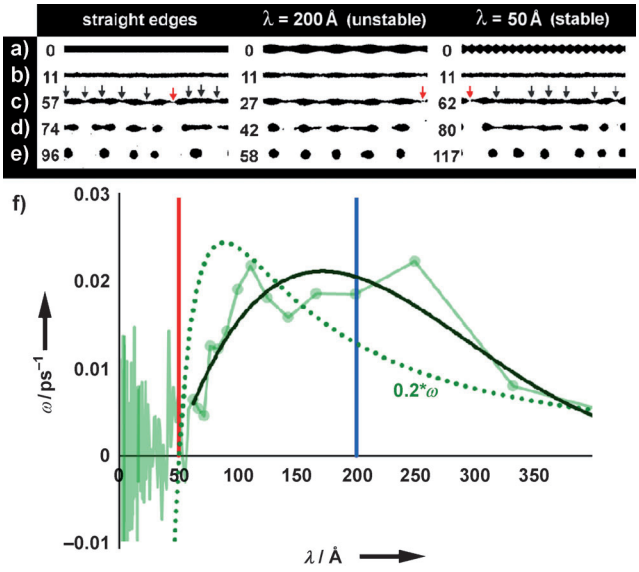

Figure 2. a)–e) Evolution of the straight (left), synthetic unstable perturbation ($\lambda = 200$ Å) (middle) and synthetic stable perturbation ($\lambda = 50$ Å) (right) for liquid Cu on solid graphite as predicted by a molecular dynamics simulation. $A_o = 7.5$ Å for both the unstable and stable modes. Black arrows: localized rivulet thinning, which predicate rivulet breakup. Red arrows: first rivulet break. Top-down images of a) the initial thin film strip, b) rivulet formation, c) the first rivulet break, d) partial breakup, and e) the nanodroplet formation time, that is, the time at which all particles are formed. The time stamps shown are in picoseconds. f) The theoretical (•••••, analytical prediction from Eq. (1) with $R_{riv} = 11.7$ Å), MD (——, ●), and MD fit (——) dispersion curves for liquid Cu resting on graphite. The analytical model curve has been reduced in growth rate by 20% ($0.2\,\omega$). An unstable mode ($\lambda = 200$ Å, blue line) and a stable mode ($\lambda = 50$ Å, red line) were selected for MD simulations.

The rivulet wetted the substrate at an angle of $\theta_{riv} = 149 \pm 4°$ (Supporting Information, S2). With knowledge of the rivulet radius R_{riv} and contact angle, the dispersion curve was estimated (Figure 2f) according to Brochard-Wyart and Redon:[10c]

$$\omega(\lambda,\theta_{riv},R_{riv}) = -\left(\frac{\theta_{riv}}{L}\right)^{4/3}\left(\frac{\eta}{\rho}\right)^{1/3}\left(\frac{\gamma}{\eta}\right)^{2/3}\frac{\left(\frac{\pi L}{\lambda}\tanh\left(\frac{\pi L}{\lambda}\right)-1\right)^{2/3}\left(1+\frac{\pi L}{\lambda}\right)^{2/3}}{\left(1+\left(\frac{\lambda}{\pi L}\right)^{2}\right)^{2/3}} \quad (1)$$

where $\omega(\lambda)$ is the varicose mode, λ the growth rate, η viscosity, ρ liquid density, γ is the liquid-vapor surface tension, and $L = 2R_o\sin\theta_{riv}$ is the contact width of the rivulet. According to the model, viscoinertial forces[13] govern the growth rate of surface perturbations on the rivulet.[10c] Unstable varicose modes are indicated by positive growth rates in Figure 2 f while stable modes have negative ω values. The model suggests a fastest growing mode of $\lambda_m = 90$ Å with a growth rate of $\omega(\lambda_m) = 0.12\ ps^{-1}$.

The self-assembly (MD simulation shown in Figure 2, left) was used to estimate a dispersion curve for the modified RP instability (Supporting Information, S3). The light green curve plotted in Figure 2 f shows the results of the fft-based analysis (Supporting Information, S3). Notably, the surface-wave spatial distribution on the rivulet at rivulet formation (11 ps) represents the initial amplitude spectrum used to derive the growth rate spectrum for the dispersion curve.

A hallmark characteristic of the RP evolution, that is, the self-assembly pathway, is the dispersion in time between breakup events located along the rivulet length. This is caused by the slight variation in growth rate between many simultaneously propagating surface waves of similar wavelength. The first rivulet breakup event takes place at $t = 57$ ps (Figure 2 c, left, red arrow), yet similar regions of local diameter minima (black arrows) also exist at $t = 57$ ps with a large variation in diameter. This phenomenon is directly attributable to the dispersion curve $\omega(\lambda)$ versus λ; although the growth rate curve has a global maximum, the maximum is not sharp and thus modes of similar wavelength compete to effect the final rivulet breakup. Moreover, growth is exponential $e^{\omega t}$ in time, and a small change in the initial amplitude of a given mode can drastically increase the influence of that mode on the rivulet breakup. The number of modes contributing to breakup also seems to increase at the nanoscale (Supporting Information, S4); that is, the MD dispersion curve FWHM is broad. This is the first difference identified between the analytical prediction and MD derived curve; for example, the growth rate at λ_m is about 80 % slower according to MD.

A global maximum in the dispersion curve typically determines the predominant mode that dictates rivulet breakup. The MD estimated dispersion curve suggests a maximum growth rate of $0.02\ ps^{-1}$ at a wavelength of about 170 Å based on the fourth-order polynomial fit to the MD simulation results (dark green line). This wavelength of maximum growth agrees well with a complementary estimate of the maximum growth rate λ_{max} calculated by determining the number of local rivulet minima N per length of rivulet L_s (Supporting Information, S5) according to L_s/N. Furthermore, as will be shown below, the growth rates estimated from the MD dispersion curve fit agree well with the results presented in Supporting Information, S6.

The final number of nanodroplets at 96 ps is 5 (Figure 2 e, straight-edged) and fewer than expected from the original estimate of the number of perturbations noted prior to the first breakup event (Figure 2 c). The merging of nanodroplets and the competing contraction of rivulet fragments into single nanodroplets changes the final particle size and pitch[7a,c,d] based on the anticipated initial distribution derived from the estimate L_s/N. This difference is also directly related to the dispersion/variation in breakup times. However, these effects can be significantly reduced by directing assembly using unstable, synthetic perturbations.

Imposing synthetic perturbations along the edges of thin film strips significantly alters both the temporal and spatial distributions of rivulet breakup. Unstable perturbations transmit to the rivulet surface, although a slight decay in amplitude occurs during the strip retraction (Figure 3). The

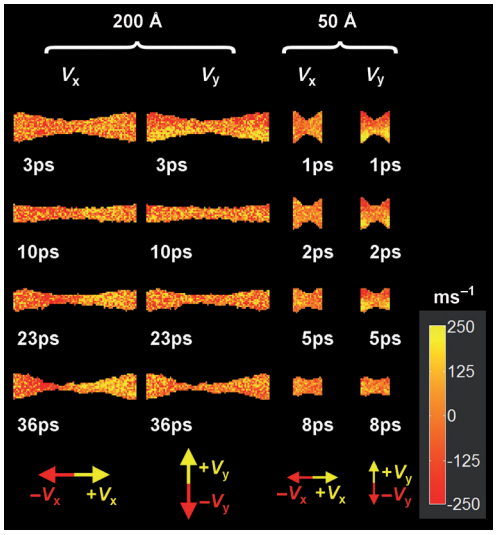

Figure 3. Averaged atomic velocity profiles, $V_x(x,y)$ and $V_y(x,y)$, demonstrating the internal velocity gradients within the rivulets at select assembly times. The evolution of the unstable ($\lambda = 200$ Å, $A_0 = 7.5$ Å) and stable cases ($\lambda = 50$ Å, $A_0 = 7.5$ Å) are shown. Local internal velocities were revealed by spatially binning the atomic velocities and averaging (Supporting Information, S8).

Cu strip with the synthetic perturbation of $\lambda = 200$ Å and $A_0 = 7.5$ Å in shown in Figure 2, middle column. The first perturbation pinches off at 27 ps (Figure 1 c) for the 200 Å case. This is significantly earlier than for the straight-edged strip (57 ps) owing to the relatively large value of A_o (7.5 Å) for the 200 Å mode. These unstable perturbations exhibit a faster rivulet breakup time owing to the relatively large initial amplitude. Synchronization of breakup in both time and space resulted as the final nanoparticle distribution at 58 ps is governed by the original synthetic varicose perturbation and the particle placement has good fidelity with the original peaks of the varicose mode.

Figure 2 a,b (right) show the original, stable synthetic perturbation morphology ($\lambda = 50$ Å, $A_0 = 7.5$ Å, and $t = 0$ ps) and the rivulet formation at 11 ps. This stable perturbation decays in 5 ps and the natural, self-assembly length scale ensues: at 62 ps (Figure 2 c, right), the first pinch-off occurs, which is delayed by 5 ps relative to the straight-edged, self-

assembly case. This is consistent with both experimental observations and continuum simulations for larger features.[7a] Also, the number of perturbations is about 8 (Figure 2c, right), which is comparable to the self-assembly case (Figure 2c, left). The positions of the evolved, natural-diameter minima located along the rivulet are clearly uncorrelated to the original synthetic perturbation, indicating the complete decay of this stable mode. Figure 2e (right) shows that the spatial distribution of nanodroplets (117 ps) is similar to the straight copper line in terms of both average pitch (ca. λ_{max}) and pitch variation. The MD-derived dispersion curve predicted both the stability (50 Å) and instability (200 Å) that was observed (Figure 2f, green line), thus providing circumstantial evidence for the validity of our method used to derive the dispersion curve (Supporting Information, S5). The RP model of rivulet breakup seems to explain a number of our observations gleaned from MD. Thus, closer examination of the underlying physics of rivulet breakup should reveal a hallmark characteristic predicted by RP theory; the mass flow away from the rivulet troughs during unstable mode growth (Supporting Information, S7). Indeed, MD captured these hydrodynamics (Figure 3).

The evolution of V_x(x,y) and V_y(x,y) for both the 50 and 200 Å cases are consistent with the mass flow profile characteristic of the RP theory. Figure 3 (200 Å case) reveals the $V_x(x,y)$ and $V_y(x,y)$ velocity profiles (clearly demonstrated at 23 and 36 ps) favoring rivulet breakup at the troughs where there is an obvious $V_x(x)$ gradient indicating mass flow out of the rivulet neck. This trend continues through 23–36 ps until breakup occurs (not shown). For the stable 50 Å case, no significant $V_x(x)$ gradient ever develops and the 50 Å perturbation decays. Figure 3 shows that synthetic perturbations both drive the formation of high-fidelity nanoparticle arrays and clearly reveal the physics driving the breakup.

Along with the exploration of the stability landscape by varying the synthetic mode wavelength, we also explored controlling the rate of directed assembly by varying the synthetic wave amplitude. It is critically important that we quantify the time increment available between stable mode decay, and unstable, directed breakup because we envisage that patterning both stable and unstable wavelengths on the same thin film strip could result in the formation of nanowires and nanoparticles in the same assembly step. An experimental example demonstrating wire/particle bistability using a larger thin film strip is shown in the Supporting Information, S9.

Lastly, specific morphological aspects of the nanoscale rivulet breakup reported herein are remarkably similar to those previously reported regarding the breakup of nanojets in free space[12,14] (Supporting Information, S10).

Even including the additional caveat of the underlying substrate for our current problem, the so-called double-cone morphology of breakup is the most often observed rivulet morphology at breakup (Figure 3, 200 Å and 36 ps), which agrees with the investigation by Moseler and Landman of a propane nanojet[12a] (Figure 3c of Ref. [12a]; Supporting Information, S10). We even observed the "small cluster, split-off" morphology, although less often, that Moseler refers to in Figure 3c of Ref. [12a] (Supporting Information, S10).

In summary, RP fluid jet destabilization, which is affected by the fluid–substrate interaction, was found to be captured using MD simulations. MD simulations showed jet stabilization and destabilization similar to that predicted by the analytical model with the additional caveat of stochastic effects. Furthermore, we aimed to investigate the scalability of self- and directed assembly of nanoparticle chains by natural RP instabilities and by patterned synthetic perturbations.[7a] MD simulations revealed that this assembly paradigm is active at the nanometer scale, where the ability to dictate jet breakup using prescribed synthetic waves was demonstrated.

Experimental Section

Molecular dynamics (MD) simulations (Supporting Information, S11) were conducted for seven unique thin film strip geometries. All of the MD calculations were performed using the software LAMMPS.[15] Common among all seven geometries were the strip length (1000 Å), thickness (10 Å), and volume (400 nm^3). The following width variations were imposed: 1) a straight edge with a width of 40 Å; 2) a varicose perturbation with a wavelength λ of 200 Å and amplitudes A_0 of 5, 7.5 and 9 Å; and 3) a $\lambda = 50$ Å perturbation with amplitudes of 5, 7.5 and 9 Å (A_o referenced in Figure 1a) while keeping the average width constant at 40 Å (Figure 1a, blue). Periodic boundary conditions[15] were implemented along the thin film strip/rivulet axis to avoid edge retraction effects which compete with the evolving, modified RP instability[7b] (Supporting Information, S11).

The Cu–Cu interaction was modeled using an embedded atom method (EAM) potential[16] while the C–C interaction was described with an adaptive intermolecular reactive empirical bond order (AIREBO)[17] potential. The C–Cu interaction was modeled using an optimum 12–6 Lennard Jones potential of well depth $\varepsilon = 0.01$ eV and a size parameter of $\sigma = 0.3225$ nm for the carbon–copper interaction.

The graphite was composed of three layers, the uppermost of which was equilibrated using the canonical ensemble (NVT) method at the same temperature as the liquid Cu; the other two graphitic layers were kept frozen. During MD simulation execution, the uppermost layer of graphite was kept at constant temperature T of 2200 K whereas the Cu strips were let to evolve freely. This temperature is a common liquid metal temperature implemented during our real PLiD experiments.[7a,18]

Received: March 16, 2012
Published online: July 29, 2012

Keywords: molecular dynamics · nanoparticles · nanotechnology · self-assembly · thin films

[1] M. H. Lee, J. Y. Lin, T. W. Odom, *Angew. Chem.* **2010**, *122*, 3121–3124; *Angew. Chem. Int. Ed.* **2010**, *49*, 3057–3060.
[2] J. Henzie, M. H. Lee, T. W. Odom, *Nat. Nanotechnol.* **2007**, *2*, 549–554.
[3] A. J. Pasquale, B. M. Reinhard, L. Dal Negro, *ACS Nano* **2011**, *5*, 6578–6585.
[4] M. T. Rahman, N. N. Shams, C. H. Lai, *J. Appl. Phys.* **2009**, *105*, 07C112.
[5] A. I. Kuznetsov, A. B. Evlyukhin, M. R. Goncalves, C. Reinhardt, A. Koroleva, M. L. Arnedillo, R. Kiyan, O. Marti, B. N. Chichkov, *ACS Nano* **2011**, *5*, 4843–4849.
[6] S. Y. Chou, Q. F. Xia, *Nat. Nanotechnol.* **2008**, *3*, 369–369.

[7] a) J. D. Fowlkes, L. Kondic, J. Diez, Y. Y. Wu, P. D. Rack, *Nano Lett.* **2011**, *11*, 2478 – 2485; b) L. Kondic, J. A. Diez, P. D. Rack, Y. F. Guan, J. D. Fowlkes, *Phys. Rev. E* **2009**, *79*, 026302; c) Y. Wu, J. D. Fowlkes, P. D. Rack, J. A. Diez, L. Kondic, *Langmuir* **2010**, *26*, 11972 – 11979; d) Y. Wu, J. D. Fowlkes, N. A. Roberts, J. A. Diez, L. Kondic, A. G. Gonzalez, P. D. Rack, *Langmuir* **2011**, *27*, 13314 – 13323; e) Y. Y. Wu, J. D. Fowlkes, P. D. Rack, J. A. Diez, L. Kondic, *Langmuir* **2010**, *26*, 11972 – 11979; f) Q. F. Xia, S. Y. Chou, *Nanotechnology* **2009**, *20*, 285310; g) J. Lian, L. M. Wang, X. C. Sun, Q. K. Yu, R. C. Ewing, *Nano Lett.* **2006**, *6*, 1047 – 1052; h) C. Favazza, R. Kalyanaraman, R. Sureshkumar, *Nanotechnology* **2006**, *17*, 4229 – 4234; i) C. Favazza, H. Krishna, R. Sureshkumar, R. Kalyanaraman, *Proc. Soc. Photo-Opt. Instrum. Eng.* **2007**, *6648*, 64809; j) C. Favazza, J. Trice, R. Kalyanaraman, R. Sureshkumar, *Appl. Phys. Lett.* **2007**, *91*, 043105; k) C. Favazza, J. Trice, H. Krishna, R. Kalyanaraman, *Proc. Soc. Photo-Opt. Instrum. Eng.* **2008**, *7039*, 3907; l) C. Favazza, J. Trice, H. Krishna, R. Kalyanaraman, *Mater. Res. Soc. Symp. Proc.* **2006**, *890*, 153 – 158; m) C. Favazza, J. Trice, H. Krishna, R. Kalyanaraman, R. Sureshkumar, *Appl. Phys. Lett.* **2006**, *88*, 153118; n) H. Krishna, C. Favazza, A. K. Gangopadhyay, R. Kalyanaraman, *JOM* **2008**, *60*, 37 – 42; o) H. Krishna, R. Sachan, J. Strader, C. Favazza, M. Khenner, R. Kalyanaraman, *Nanotechnology* **2010**, *21*, 155601; p) N. Shirato, H. Krishna, R. Kalyanaraman, *J. Appl. Phys.* **2010**, *108*, 024313; q) J. Trice, D. Thomas, C. Favazza, R. Sureshkumar, R. Kalyanaraman, *Phys. Rev. B* **2007**, *75*, 235439.

[8] a) A. Vrij, J. T. Overbeek, *J. Am. Chem. Soc.* **1968**, *90*, 3074 – 3078; b) R. Seemann, S. Herminghaus, K. Jacobs, *Phys. Rev. Lett.* **2001**, *86*, 5534 – 5537; c) J. Becker, G. Grun, R. Seemann, H. Mantz, K. Jacobs, K. R. Mecke, R. Blossey, *Nat. Mater.* **2003**, *2*, 59 – 63.

[9] a) L. Rayleigh, *Philos. Magazine Ser. 5* **1892**, *34*, 145 – 154; b) J. A. F. Plateau, *Acad. Sci. Brux. Mem.* **1843**, *16*, 3.

[10] a) J. A. Diez, A. G. Gonzalez, L. Kondic, *Phys. Fluids* **2009**, *21*, 082105; b) K. Sekimoto, R. Oguma, K. Kawasaki, *Ann. Phys. New York* **1987**, *176*, 359 – 392; c) F. Brochard-Wyart, C. Redon, *Langmuir* **1992**, *8*, 2324 – 2329.

[11] D. Bonn, J. Eggers, J. Indekeu, J. Meunier, E. Rolley, *Rev. Mod. Phys.* **2009**, *81*, 739 – 805.

[12] a) M. Moseler, U. Landman, *Science* **2000**, *289*, 1165 – 1169; b) J. Eggers, *Phys. Rev. Lett.* **2002**, *89*, 084502.

[13] a) D. Bartolo, C. Josserand, D. Bonn, *J. Fluid Mech.* **2005**, *545*, 329 – 338; b) C. Andrieu, C. Sykes, F. Brochard, *J. Adhes.* **1996**, *58*, 15 – 24.

[14] J. Eggers, E. Villermaux, *Rep. Prog. Phys.* **2008**, *71*, 036601.

[15] S. Plimpton, *J. Comput. Phys.* **1995**, *117*, 1 – 19.

[16] a) M. S. Daw, M. I. Baskes, *Phys. Rev. B* **1984**, *29*, 6443 – 6453; b) M. S. Daw, M. I. Baskes, *Phys. Rev. Lett.* **1983**, *50*, 1285 – 1288; c) M. S. Daw, S. M. Foiles, M. I. Baskes, *Mater. Sci. Rep.* **1993**, *9*, 251 – 310.

[17] S. J. Stuart, A. B. Tutein, J. A. Harrison, *J. Chem. Phys.* **2000**, *112*, 6472 – 6486.

[18] a) M. Fuentes-Cabrera, B. H. Rhodes, J. D. Fowlkes, A. Lopez-Benzanilla, H. Terrones, M. L. Simpson, P. D. Rack, *Phys. Rev. E* **2011**, *83*, 041603; b) Y. V. Naidich, G. A. A. Kolesnichenko, *Powder Metall. Met. Ceram.* **1968**, *7*, 3.

